# Power Loss Modes of BIPV Modules: An Analytical Approach Using Outdoor I-V Curves

Abdulkerim Gok, Ebrar Ozkalay, Gabi Friesen, and Francesco Frontini

***Abstract*—Using outdoor time-series I-V curves, the Analytic $I_{sc}$-$V_{oc}$ method was applied to glass/backsheet and glass/glass c-Si module constructions with ventilated and insulated mounting configurations in order to explore contributing factors to degradation in power performance. The rates of power loss modes; namely uniform current, recombination, series resistance, and current mismatch, were assessed for each module and configuration. The effect of thermal insulation was evident in the glass/backsheet module with an EVA type encapsulant: the observed loss in performance was chiefly originated from the resistive loss. The cell and metallization defects induced by thermo-mechanical stresses were believed to be main reasons. However, the double glass module with a PVB type encapsulant was more resistant to thermal effects: a large increase in the uniform current, compensated by the resistive loss, was the main driver for the observed gain in performance. For all modules and configurations, the calculated power loss mode rates were compared with the reported performance loss rates and they were found to be in close agreement. This analytic technique was found to be a powerful method in order to determine and quantify the individual contributions from specific power loss modes to overall module performance.**

***Index Terms*—building integrated photovoltaics (BIPV); outdoor I-V curves; power loss modes; the analytic $I_{sc}$-$V_{oc}$ method; year-over-year (YoY) regression; thermal insulation**

## I. Introduction

Solar photovoltaic (PV) energy is one of the most cleanest and abundant sources of renewable energy. Thanks to reduction in cost, advances in technology, improved competitiveness against fossil fuels, and continuous policy support, PV installations have shown a tremendous growth in recent years. The share of PV in global electricity generation is expected to have increased approximately by 15 % reaching a total installed capacity of 734 GW worldwide with the addition of 107 GW (estimated in the main case) in 2020 [1]. The application of building-integrated photovoltaic (BIPV) systems is one of the key research areas in order to achieve nearly zero energy buildings and reduce greenhouse gas emissions [2], [3]. BIPV systems can also provide reduction in both energy and material costs by replacing conventional building envelope [4], [5]. Operating temperature is, however, one of most important factors for electrical and thermal performances of BIPV modules [6], [7]. Unlike the ground-mounted systems, BIPV modules are installed as part of the building envelope, leading to reduced or no ventilation on the rear side, especially in rooftop applications. Convective heat transfer caused by wind in this case is restricted, resulting in elevated operating temperatures.

In PV reliability research, degradation mechanisms such as discoloration, delamination, backsheet defects, cell cracks, metallization failures, etc., are often reported during outdoor service and indoor weathering experiments in order to explore the effect of environmental stress factors on the service lifetime of PV modules. Depending on the cell technology, module construction, mounting configuration, and climatic conditions such as solar irradiance, ambient temperature, and wind speed and direction, power loss modes can differ during outdoor service. Performance loss rate (PLR) calculations are performed using the module maximum power in order to assess quantitative information about the overall module performance [8], [9]. However, PLR does not constitute information about the contributing factors to degradation in performance. Changes in the rates of I-V curve parameters, such as $V_{oc}$, $I_{sc}$, and fill factor (FF), can provide additional aspects about the module characteristics [10], but they do not possess information about the physical loss mechanisms that are directly related to the power performance and are affected by parasitic resistances.

The Suns-$V_{oc}$ method [11], [12], [13], on the other hand, can be applied to construct resistance-free I-V curves and thus explore additional insight for individual power loss modes. In this method, simultaneous $V_{oc}$ measurements are taken under varying incident light intensities from 0.1 sun to several suns intensity. With this method, both cell- and module-level measurements can be implemented using transient and quasi-static illumination conditions [14], [15]. The determination of non-uniform power loss modes can then be established in a quantitative way by comparing I-V curves with Suns-$V_{oc}$ curves. Suns-$V_{oc}$ curves are usually constructed under well-controlled indoor measurements, but it can be applied to outdoor data as well with proper temperature and irradiance correction [16], [17], [18], [19]. Toward this purpose, a method

This work was partially supported by the Swiss National Science Foundation under COST IZCOZ0_182967/1. The work of A. Gok was supported by a Grant from the COST Action PEARL PV Project (CA 61235—Performance and Reliability of Photovoltaic Systems: Evaluations of Large-Scale Monitoring Data) for the Short-Term Scientific Mission at the University of Applied Sciences and Arts of Southern Switzerland (SUPSI).

A. Gok is with the Department of Materials Science and Engineering, Gebze Technical University, Gebze, Kocaeli, 41400 Turkey (e-mail: agok@gtu.edu.tr).

E. Ozkalay, G. Friesen, and F. Frontini are with the Department for Environment Constructions and Design, University of Applied Sciences and Arts of Southern Switzerland (SUPSI), Canobbio, CH-6952, Switzerland (e-mail: ebrar.oezkalay@supsi.ch; gabi.friesen@supsi.ch; francesco.frontini@supsi.ch).

Manuscript received MM-DD-YYYY; revised MM-DD-YYYY.

called Analytic $I_{sc}$-$V_{oc}$ has been developed and applied to outdoor time-series I-V curves for more detailed analysis of specific power loss modes contributing to overall performance behavior of PV modules [20], [21], [22].

In this paper, the Analytic $I_{sc}$-$V_{oc}$ method was applied to two different crystalline silicon (c-Si) BIPV module constructions with two different mounting configurations in order to explore additional information about the effect of thermal insulation on the module performances. Power loss modes, that are uniform current, recombination, series resistance, and current mismatch, were determined quantitatively for each module and mounting configuration. Year-over-Year (YoY) regression was applied to each power loss mode in order to obtain comparable rates, i.e., power loss mode rates, to the reported performance loss rates. The possible causes for the observed power loss modes and their effects on the overall performance of the modules were further discussed.

## II. Methodology

### A. Modules and Mounting Configurations

The performances of glass/backsheet (G/B) and glass/glass (G/G) modules with open-rack for ventilated and thermally insulated on the rear for non-ventilated (insulated) configurations were monitored for more than four years in Canobbio, Switzerland, a Cfb Köppen-Geiger climate zone. Both module types are frameless, commercial modules, consisting of serially connected c-Si Al-BSF cells (66 cells with three busbars in G/B and 64 cells with two busbars in G/G) with three bypass-diodes. The G/B module construction is composed of an ethylene-vinyl acetate (EVA) type encapsulant and a fluoropolymer type backsheet. The double glass G/G module construction, however, comprises a polyvinyl-butyral (PVB) type encapsulant. Both encapsulant materials are standard clear films on both front and rear cell sides with no particular UV barrier. For the insulated configuration, 20 cm thick polyurethane layer was used to demonstrate the thermal insulation effect. Modules were glued on their backside using single-component structural silicone adhesive. The modules were mounted on a fixed rack with a tilt angle of 6° and a sun azimuth of -4° from the South. The latitude and longitude of the installation site are 46.02 °N and 8.91 °E, respectively.

In our previous work [23], evaluations of the performance loss rates (PLR) of these modules were demonstrated for module performance ratio (MPR) parameter using the module maximum power ($P_{mp}$) and other I-V curve parameters such as $I_{sc}$, $V_{oc}$, and fill factor (FF). Evolutions of the daily-averaged insolation-weighted performance rates for each parameter were included along with the PLR fitting curves obtained through the YoY methodology. Modules and the corresponding PLR values are reported in Table I for each parameter.

### B. Data Collection

Module performance parameters including time-series maximum power, voltage and current, and time-series full I-V curves were acquired using an in-house MPPT3000 tracer at 5-min intervals between February 2014 and July 2018. This tracer works in an auto-range mode adapting I/V ranges depending on the irradiance level. Considering the modules' maximum I/V values, corresponding ranges were taken as 50V/10A with an accuracy level of 0.2 % at full scale. Module temperatures were measured using thermocouples attached on the back surface of the modules. The daily-averaged insolation-weighted module temperatures can be seen in Fig. 1. Thermal insulation effect is evident as there is approximately 25°C difference between the ventilated and insulated mounting configurations regardless of the module construction. The plane of array ($G_{POA}$) irradiance data was collected using a single calibrated pyranometer installed on the same plane as modules. Series resistance values, which are required for the power loss mode analysis, were obtained using the data-driven I-V curve extraction method (ddiv) [24], [25].

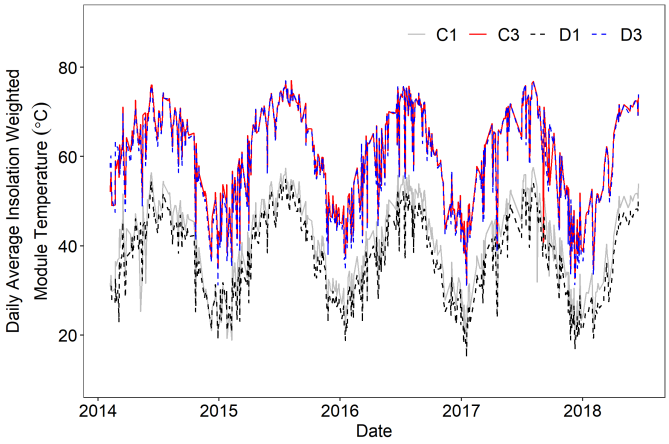


Fig. 1: Measured Module Operating Temperatures

### C. The Analytic $I_{sc}$-$V_{oc}$ Method

For power loss mode calculations, the Analytic $I_{sc}$-$V_{oc}$ method [21] was applied in this work. This method first determines the reference temperature and irradiance conditions and translates I-V curve parameters to these reference conditions, then prepares pseudo I-V curves for every data analysis period. The differences between the pseudo I-V curves and the real I-V curves reveal the power loss modes.

Since the module temperature of 25°C under the irradiance of 1000 $\mathrm{Wm}^{-2}$, defined by the standard testing conditions (STC), is not realistic, the reference temperature condition ($T_{m,RC}$) is obtained from the measured module temperatures. $T_{m,RC}$ is determined as the median module temperature between the irradiance of 995 and 1005 $\mathrm{Wm}^{-2}$.

As explained in Ref. [21], a dynamic data-driven modelling approach is used to determine the physical parameters of the models for each analysis period. First, the $V_{oc}$ values are corrected to the reference temperature condition. By neglecting the temperature coefficient of $I_{sc}$, $V_{oc}$, which is a function of $I_{sc}$ and temperature, is obtained by the Sandia's Photovoltaic Array Performance model [26] as follows:

$$V_{oc}(I_{sc}, T_m) = \alpha_0 + \alpha_1 \cdot T_m \cdot \ln I_{sc} + \alpha_2 \cdot T_m + \epsilon \quad (1)$$

TABLE I: Performance Loss Rates (PLR) of the Modules

| **Parameters** | **Modules** | | | |
|---|---|---|---|---|
| | C1 Ventilated G/B | C3 Insulated G/B | D1 Ventilated G/G | D3 Insulated G/G |
| MPR (%/yr) | 0.01 | -0.42 | -0.10 | 0.26 |
| $V_{oc}$ (%/yr) | 0.03 | -0.04 | -0.04 | 0.07 |
| $I_{sc}$ (%/yr) | -0.08 | -0.01 | 0.02 | 0.42 |
| FF (%/yr) | 0.06 | -0.26 | -0.01 | -0.21 |

where $T_m$ is the measured module temperature in Kelvin, $\alpha_i$ $(i = 0, 1, 2)$ are the fitting coefficients of the model, and $\epsilon$ is the error term.

Similarly, the simple linear relationship between $I_{sc}$ and irradiance can be expressed as follows:

$$I_{sc}(G_{POA}) = \kappa \times G_{POA} + \epsilon \tag{2}$$

where $\kappa$ is the fitting coefficient of the model. The reference $I_{sc}$ condition ($I_{sc,RC}$) is then determined at the irradiance of 1000 $Wm^{-2}$ for one sun intensity.

In order to construct the Analytic $I_{sc}$-$V_{oc}$ curves, temperature-corrected $V_{oc}$ values are paired with varying $I_{sc}$ values. Then, the pseudo I-V curves are built following the principle of superposition. The current values in the pseudo I-V curves ($I_{psd}$) are calculated using the varying current ($I_{sc}$) values in the Analytic $I_{sc}$-$V_{oc}$ curves as follows:

$$I_{psd} = I_{sc,RC} - I_{sc} \tag{3}$$

For power loss mode calculations, both pseudo I-V and real I-V curves must be at the reference conditions. Instead of correcting the entire I-V curve, only certain extracted key features, such as $I_{mp}$, $V_{mp}$, and $R_s$, are corrected to the reference temperature and irradiance conditions with the following physics-based equations:

$$I_{mp}(I_{sc}, T_m) = \beta_0 + \beta_1 \cdot T_m \cdot I_{sc} + \beta_2 \cdot T_m \cdot I_{sc}^2 + \epsilon \tag{4}$$

$$\begin{aligned} V_{mp}(I_{sc}, T_m) = \gamma_0 + \gamma_1 \cdot T_m \cdot \ln I_{sc} \\ + \gamma_2 \cdot (T_m \cdot \ln I_{sc})^2 + \gamma_3 \cdot T_m + \epsilon \end{aligned} \tag{5}$$

$$R_s(I_{sc}, T_m) = \delta_0 + \delta_1 \cdot \frac{T_m}{I_{sc}} + \epsilon \tag{6}$$

where $\beta_i (i = 0, 1, 2)$, $\gamma_i (i = 0, 1, 2, 3)$, and $\delta_i (i = 0, 1)$ are the fitting coefficients of the models. For the reference conditions corrected $I_{mp}$, $V_{mp}$, and $R_s$ values, $T_{m,RC}$ and $I_{sc,RC}$ are substituted into (4)-(6) for each analysis period.

For power loss mode calculations, two pseudo I-V curves are created for each analysis period. One (initial) pseudo I-V curve is constructed at the beginning of the analysis period (undegraded) and the other pseudo I-V curve is constructed after each analysis period (degraded). There are four different power loss modes investigated in this analysis: uniform current, recombination, series resistance, and current mismatch.

Uniform current loss is mainly related to the amount of light reaching the solar cells. In order to determine uniform current loss, $I_{sc}$ corrected pseudo I-V curve is first derived using (7) on every $I_{sc}$ values of the initial pseudo I-V curve as follows:

$$I_{corr} = I_{init} - \Delta I_{sc} \tag{7}$$

where $I_{corr}$ is the current values of the $I_{sc}$ corrected pseudo I-V curve, $I_{init}$ is the current values of the initial pseudo I-V curve, and $\Delta I_{sc}$ is the difference between $I_{sc}$ values of the initial and degraded pseudo I-V curves. Voltage values of the $I_{sc}$ corrected pseudo I-V curve remain the same with that of the initial pseudo I-V curve. The amount of uniform current loss through each analysis period is then calculated from the $P_{mp}$ difference between the initial pseudo and $I_{sc}$ corrected pseudo I-V curves.

Recombination loss is a measure of degradation in $V_{oc}$. It is obtained from the $P_{mp}$ difference between the $I_{sc}$ corrected pseudo and degraded pseudo I-V curves.

Resistive loss is mostly induced by defective cells and metallization such as cracked or broken cells, interrupted or corroded metallization elements. In order to determine resistive loss, $R_s$ correction is first applied to the degraded pseudo I-V curve by using (8) on every voltage values on the curve while keeping the current values the same as follows:

$$V_{corr} = V_{dPIV} + I \cdot R_{s,dPIV} - I \cdot R_{s,IV} \tag{8}$$

where $V_{corr}$ is the voltage values of the $R_s$ corrected degraded pseudo I-V curve, $V_{dPIV}$ is the voltage values of the degraded pseudo I-V curve, $R_{s,\,dPIV}$ is the series resistance of the degraded pseudo I-V curve, and $R_{s,\,IV}$ is the series resistance of the real I-V curve. The $P_{mp}$ difference between the degraded pseudo and $R_s$ corrected degraded pseudo I-V curves then yields the resistive loss.

Current mismatch loss is chiefly related to activation of bypass diodes due to transient changes like partial shading or loose electrical connection, or permanent changes like cell cracks. It is obtained from the $P_{mp}$ difference between the $R_s$ corrected degraded pseudo I-V and real I-V curves.

A process chart for extracting these power loss modes from the constructed pseudo I-V curves is shown in Fig. 2.

### *D. Data Filtering*

In PLR calculation for degradation rate analysis, filtering for irradiance is usually applied for low, i.e., $<$250 $\mathrm{Wm}^{-2}$, and high, i.e., $>$1250 $\mathrm{Wm}^{-2}$, irradiance levels. Clear sky index is

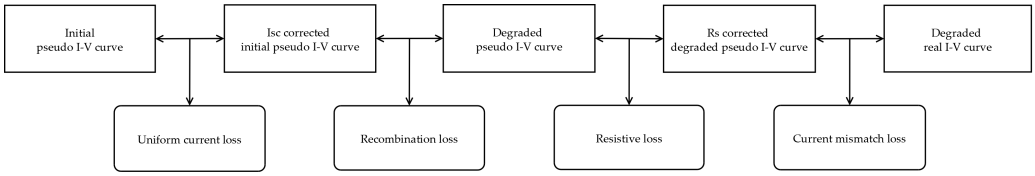


Fig. 2: Extraction of Power Loss Modes from the Constructed Pseudo I-V Curves

also used for further filtering in order to avoid irregularities in irradiance data caused by ground-based sensors. This process makes the PLR calculation easier, but results in lesser amount of data. In order to keep more information on modules and power loss modes, intensive irradiance filtering is avoided in this analysis. All the data greater than the tracer's accuracy level was therefore utilized, i.e., I-V curves with $I_{sc}$ greater than 0.02 A and $V_{oc}$ greater than 0.1 V. Considering the daytime data (average of 4.5 hours of daylight on the installation site per day) with a 5-min interval for over four years, this filtering procedure led to around 125,000 I-V curves for each module. In order to construct $I_{sc}$-$V_{oc}$ curves with high precision, analysis period was selected as 7-days. This period yielded 200 to 600 data points for one $I_{sc}$-$V_{oc}$ curve depending on the number of observations in the relevant time period.

### *E. Calculation of the Power Loss Mode Rates*

Rates for the power loss modes were determined using the YoY regression [27] for comparison with the previously reported PLR of the module parameters. In YoY regression of this weekly data, the rate of change between two data points in the same week of subsequent years was calculated by a linear regression model. The slopes obtained from these models formed a distribution and the estimate of the central-difference, i.e., median of the slopes, then produced the rate of change per year for a loss mode of interest. Since the power loss modes determined from this Analytic $I_{sc}$-$V_{oc}$ method are in terms of loss in power ($\Delta$W), the obtained rates in W/yr were converted to %/yr by normalizing with the initial predicted maximum power of each module. Compared to the standard least square regression, YoY is a more robust method in case of seasonal data and it is insensitive to outliers [28]. Rates with low uncertainty can easily be obtained with at least two years of data. The 95 % bias-corrected, accelerated confidence intervals ($BC_aCI$) were finally calculated for each loss mode rate using the bootstrap method based on 10,000 iterations.

## III. Results and Discussion

### *A. Evaluation of the Models*

Statistical metrics including adjusted-$R^2$ and root mean squared error (RMSE) values of the constructed models are reported in Table II for $V_{oc}$, $V_{mp}$, $I_{sc}$, $I_{mp}$, $R_s$, and the ideality factor ($n$) parameters. It is to be noted that these metrics are median values with the corresponding standard deviations because the models were fitted for each analysis period of 7-days. Since $P_{mp}$ is not modeled, but taken as the product of predicted values of $V_{mp}$ and $I_{mp}$, no adjusted-$R^2$ values were reported. Other than $R_s$, all the I-V curve parameters show adjusted-$R^2$ values greater than 0.98 with relatively small standard deviations. Since a data-driven approach was utilized to extract $R_s$ values, i.e., negative inverse slope of the I-V curve near $V_{oc}$, large changes in current values in the linear part of the I-V curves near $V_{oc}$ led to adjusted-$R^2$ values of around 0.80 for $R_s$ with relatively large standard deviations.

### *B. Evolution of the Power Loss Modes*

It is to be noted that power loss modes with instantaneous positive rates do not necessarily indicate an increase in power, but the power at the reference conditions of one sun irradiance and a median module temperatures. This could be due to mismatch in sensor readings from both the pyranometer and thermocouples. For example, if the measured $G_{POA}$ data is different from the actual $G_{POA}$, then this results in a shift between the predicted and actual power at the reference conditions. The same holds true for the temperature measurements as well when correcting the I-V curve parameters.

The evolution of power loss modes of the G/B type modules are shown in Fig. 3 with loss mode rates. The ventilated C1 module exhibits a larger uniform current loss rate (-0.22 %/yr) than the insulated C3 module (-0.07 %/yr). For the recombination losses, both modules show negligible rates with the ventilated C1 module having a greater rate (0.09 %/yr) than the insulated C3 module (-0.01%/yr). The effect of thermal insulation is evident from the resistive and current mismatch losses. While the ventilated C1 module shows a very small resistive loss rate (-0.06 %/yr), the insulated C3 module experiences a pronounced increase in the resistive loss (-0.36 %/yr). Similarly, the insulated C3 module displays quite larger current mismatch loss rate (-0.30 %/yr) than the ventilated C1 module (0.17 %/yr).

The evolution of power loss modes of the G/G (double glass) type modules are shown in Fig. 4 with loss mode rates. While the ventilated D1 module exhibits a slight decrease in the uniform current (-0.07 %/yr), the insulated D3 module experiences a marked increase with a substantial positive rate (0.40 %/yr). For the recombination loss, both modules show small rates, similar to the G/B type modules, with the insulated D3 module having a greater rate (0.11 %/yr) than the ventilated D1 module (0.01%/yr). The rate for the resistive loss is larger in the insulated D3 module (-0.22 %/yr) than that in the ventilated D1 module (-0.17 %/yr) as expected from the increased resistance when insulated. Similarly, the insulated D3 module depicts larger current mismatch loss rate (-0.09 %/yr) than the ventilated D1 module (0.17 %/yr).

TABLE II: Statistical Metrics for the Fitted Models of the Module Parameters

| **Parameters** | **Metrics** | **Modules** | | | |
|---|---|---|---|---|---|
| | | C1 | C3 | D1 | D3 |
| $V_{oc}$ | adj-$R^2$ | 0.991 ± 0.106 | 0.995 ± 0.125 | 0.983 ± 0.161 | 0.994 ± 0.111 |
| | RMSE | 0.094 ± 0.219 | 0.096 ± 0.317 | 0.126 ± 0.416 | 0.111 ± 0.314 |
| $V_{mp}$ | adj-$R^2$ | 0.990 ± 0.049 | 0.997 ± 0.070 | 0.993 ± 0.095 | 0.998 ± 0.044 |
| | RMSE | 0.119 ± 0.138 | 0.108 ± 0.286 | 0.089 ± 0.262 | 0.089 ± 0.198 |
| $I_{sc}$ | adj-$R^2$ | 0.988 ± 0.019 | 0.988 ± 0.019 | 0.988 ± 0.018 | 0.987 ± 0.018 |
| | RMSE | 0.282 ± 0.157 | 0.273 ± 0.161 | 0.178 ± 0.106 | 0.182 ± 0.103 |
| $I_{mp}$ | adj-$R^2$ | 1.000 ± 0.001 | 1.000 ± 0.001 | 1.000 ± 0.000 | 1.000 ± 0.001 |
| | RMSE | 0.025 ± 0.041 | 0.022 ± 0.031 | 0.012 ± 0.012 | 0.017 ± 0.018 |
| $R_s$ | adj-$R^2$ | 0.885 ± 0.200 | 0.741 ± 0.263 | 0.854 ± 0.197 | 0.782 ± 0.196 |
| | RMSE | 0.063 ± 0.077 | 0.089 ± 0.131 | 0.060 ± 0.075 | 0.074 ± 0.065 |
| Fitted $n$ | | 1.151 ± 0.068 | 1.073 ± 0.084 | 1.008 ± 0.103 | 1.037 ± 0.077 |

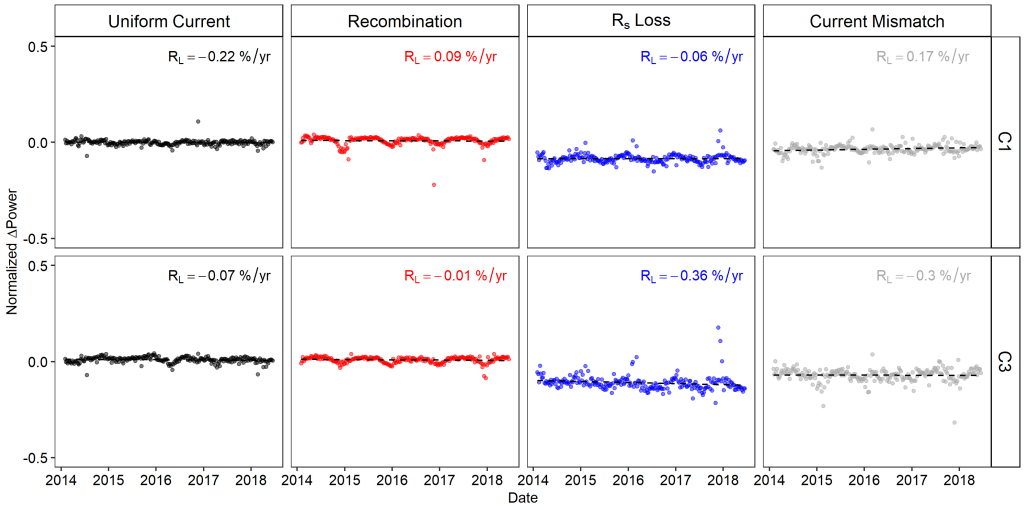


Fig. 3: Evolution of the Power Loss Modes of the G/B Type (Ventilated C1 and Insulated C3) Module Construction

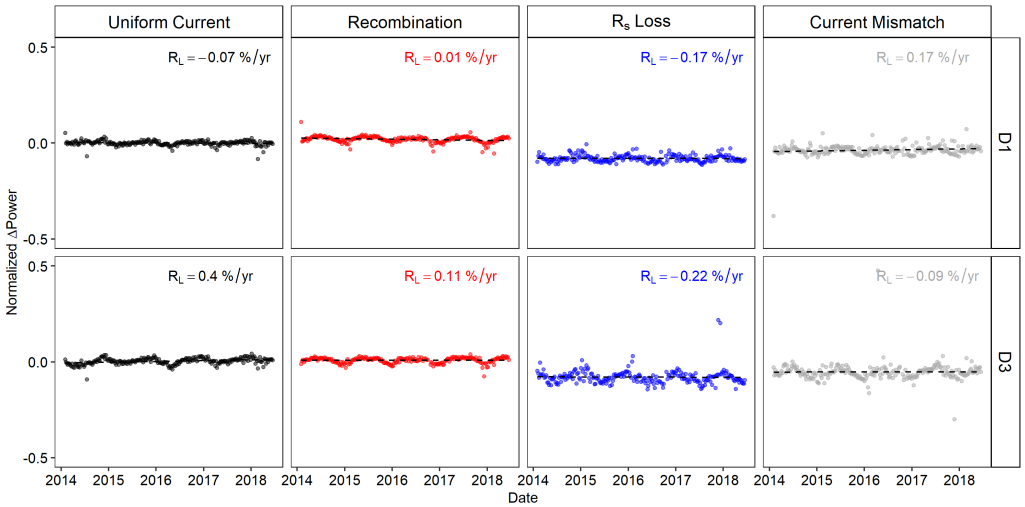


Fig. 4: Evolution of the Power Loss Modes of the G/G Type (Ventilated D1 and Insulated D3) Module Construction

### C. Power Loss Modes and Degradation Mechanisms

In this analytical method, each power loss mode indicates its individual contribution to overall performance behavior of the modules. In order for them to be directly comparable to the PLR values of the modules that are reported in Table I, each loss mode was also converted from loss in power (in watts) to % change per year by normalizing the data by the initial predicted maximum power. It is to be noted that power loss mode rate is the rate of change in particular power loss mode such as uniform current, recombination, series resistance, and current mismatch, and performance loss rate (PLR) is the rate of change in particular performance metric such as $P_{mp}$, $I_{sc}$, $V_{oc}$, and fill factor (FF). The confidence intervals and standard errors for the calculated loss mode rates are provided in Table III for each module.

Uniform current loss is characterized by the reduction in $I_{sc}$ which can be induced by soiling, snow coverage, uniform shading, and discoloration of the encapsulant. While discoloration is a permanent degradation mechanism, others are transient and can be resolved by regular cleaning of the module surface. Degradation of EVA through thermal and photo-oxidative reactions is known to result in yellow appearance leading to decreased light transmittance to the cells and performance loss [29]. In this study, all modules experienced the same environmental conditions without manual surface cleaning. The tilt angle of 6° was applied to enable natural cleaning by occasional rainfall. Considering the small uniform current loss rates in the G/B type modules, soiling by accumulation of dirt on the modules' surfaces is more likely than the discoloration of the encapsulant.

On the other hand, the marked increase in the uniform current in the insulated D3 module points out the role of the PVB type encapsulant in the G/G module construction when insulated. Softening of the PVB polymer, which is an amorphous polymer with high viscosity, is known to occur at elevated temperatures [30], that can induce morphological changes in the polymer structure such as decreased crystallinity and thus lead to increased light transmittance to the PV cells. Factors affecting the performance of c-Si modules under the effect of back thermal insulation such as module temperature, angle of incidence, and solar reflectance or transmittance have been found to be related to the module packaging components [31]. Therefore, the mechanism for improved transmittance of PVB encapsulant and thus higher current in this insulated G/G module construction should further be elucidated. The reported PLR values of the $I_{sc}$ parameter are in close agreement with the calculated uniform current loss rates of all modules and especially support the finding about the insulated D3 module.

Recombination loss is a measure of degradation in the $V_{oc}$ parameter and mostly indicates long-term performance degradation. $V_{oc}$ has a negative temperature coefficient and hence decreases with increasing temperature. However, the dissociation of boron-oxygen (B-O) defects in c-Si cells, which normally reduce the minority carrier lifetime by acting as recombination center, arisen during recovery from light induced degradation (LID), or light-induced regeneration (LIR), has been found to lead to an increased $V_{oc}$ [32], [33]. Deactivation of these B-O complexes has also been observed during outdoor deployment under the combined effect of illumination and temperature [34]. This phenomenon could explain the positive rates observed for the ventilated C1 and insulated D3 modules. Within the operating temperature range (up to $\sim$ 90°C), all modules, however, show only small recombination loss rates similar to the reported PLR values of the $V_{oc}$ parameter.

Resistive loss, mainly caused by defective cells and metallization, indicates permanent and long-term degradation and largely affects the fill factor parameter. The effect of thermal insulation in the C3 module is evident from the marked decrease in power when compared to the ventilated C1 module. Temperature induced mechanical stresses in the insulated module could be the cause for this behavior. As reported in Ref. [23], aggregated stress levels at the cell/encapsulant interface led to noticeable micro-crack formation in the insulated C3 module. Moreover, EVA releases corrosive acetic acid when degraded under hydrolytic conditions [35] that reacts with metallization and results in a decreased performance. Increase in temperature further accelerates this process. The PLR values of the fill factor parameters reflect the observed resistive losses in these G/B modules.

The situation is similar in the double glass modules. The rate of resistive loss of the insulated D3 module is larger than that of the ventilated D1 module. Moreover, this observation is also supported by the PLR values of the fill factor parameters, especially for the insulated D3 modules. However, when

TABLE III: Power Loss Mode Rates ($R_L$) with 95 % confidence intervals (CI)

| **Loss modes** | **Loss rates** | **Modules** | | | |
|---|---|---|---|---|---|
| | | C1 | C3 | D1 | D3 |
| Uniform current | $R_L$ (%/yr) | -0.22 ± 0.14 | -0.07 ± 0.14 | -0.07 ± 0.09 | 0.40 ± 0.17 |
| | CI (%/yr) | -0.37 to -0.09 | -0.22 to 0.05 | -0.21 to -0.03 | 0.22 to 0.55 |
| Recombination | $R_L$ (%/yr) | 0.09 ± 0.08 | -0.01 ± 0.07 | 0.01 ± 0.14 | 0.11 ± 0.09 |
| | CI (%/yr) | -0.04 to 0.15 | -0.08 to 0.05 | -0.20 to 0.08 | 0.03 to 0.21 |
| Series resistance | $R_L$ (%/yr) | -0.06 ± 0.11 | -0.36 ± 0.33 | -0.17 ± 0.17 | -0.22 ± 0.19 |
| | CI (%/yr) | -0.15 to 0.08 | -0.82 to -0.01 | -0.38 to -0.02 | -0.45 to -0.06 |
| Current mismatch | $R_L$ (%/yr) | 0.17 ± 0.24 | -0.30 ± 0.26 | 0.17 ± 0.15 | -0.09 ± 0.22 |
| | CI (%/yr) | -0.05 to 0.41 | -0.51 to -0.07 | 0.02 to 0.25 | -0.37 to 0.06 |

compared the insulated C3 and D3 modules, the G/G module is seen to be affected by resistive losses less than the G/B module. This can infer that the double glass construction is more resilient against temperature induced mechanical stresses caused by the thermal expansion coefficient mismatch. The observed resistive losses could be related to finger-grid failures observed in these G/G modules (as observed by the EL characterization in Ref. [23]). These finger interruptions were attributed to the softening of the PVB polymer with increased temperature [23] that can lead to a decreased shear strength and an increased creep [36]. Consequently, softening of the encapsulant layer could result in stressed cells and cell interconnects. The maximum temperature of around 90°C reached in this module construction when insulated is much higher than the glass transition temperature of the PVB polymer ($\sim$ 20°C [37]). Therefore, the formation of these finger-grid failures can be accelerated by the lateral thermal gradients between the module interfaces, e.g., between the cell and encapsulant layers.

Current mismatch loss can be a sign of transient changes in module performance like partial shading or loose electrical connection or permanent changes like cell cracks. Particularly, the presence of inactive cell areas in the insulated C3 module (as observed by the EL characterization in Ref. [23]) induced by the damaged cell interconnects due to thermally induced stresses could be in effect for the observed current mismatch loss. However, the insulated D3 module is seen to be affected less than the insulated C3 module. This was also evidenced by the larger inactive cell areas in the insulated C3 module compared to the insulated D3 modules. The damaged cell interconnects could also be the reason for the increased resistive loss in the insulated C3 module. On the other hand, positive current mismatch loss rates observed for the ventilated C1 and D1 modules could be caused by decreased current. These ventilated modules do not carry any indication of failures such as loose electrical connection or cell cracks (as observed by the EL characterization in Ref. [23]) that would cause mismatch current loss and activate the bypass-diodes.

For overall performance evaluation of the insulated modules, the PLR of module performance ratios (MPR), determined using the module maximum power ($P_{mp}$) parameter, can be a useful metric. The marked degradation in the insulated C3 module with an MPR of -0.42 %/yr is driven by the resistive loss, which is reflected by the loss in fill factor, at elevated operating temperature. However, the gain in performance in the insulated D3 module with an MPR of 0.26 %/yr is a result of the increased uniform current combined with the resistive loss. As reported in Ref. [23], these two competing mechanisms affect the power performance concomitantly. The large increase in uniform current under the influence of resistive loss which caused a loss in fill factor led to a moderate increase in power performance.

It is to be noted that the G/G and G/B modules examined in this work are not identically produced; their manufacturers, encapsulant materials they consisted of, the size of the modules, and the number of cells in each type, etc. are different. If the only difference between these module constructions were the rear layer (glass or polymeric backsheet), perhaps it would be safe to make a solid argument about the performance of one type over the other. Therefore, the observed gain in performance in the G/G module when thermally insulated may not be extrapolated to any double glass module case and may not necessarily mean that G/G modules are more stable than the G/B modules.

## IV. Conclusion

In this paper, the application of the Analytic $I_{sc}$-$V_{oc}$ method was demonstrated using the outdoor time-series I-V curves. Individual power loss modes were determined and quantified in order to elucidate the contributing factors to overall performance of different module constructions under the effect of thermal insulation. Resistive loss was found to be the dominant power loss mode in both glass/backsheet and glass/glass modules due to cell and metallization defects induced by increased operating temperatures affecting the fill factor. However, a large gain in uniform current in the glass/glass construction with a PVB type encapsulant led to an increased power performance. This finding points out the importance of the role of module construction and packaging materials for long-term performance. The calculated rates of the observed power loss modes were found to be in line with the reported performance loss rates. Compared to traditional methods for performance evaluation, this data-driven method utilizing outdoor time-series I-V curves is a powerful technique to extract additional information about the contributions factors to observed losses (or gains) in performance. With this method, outdoor I-V curves can be properly translated to environmental conditions that they are exposed to and therefore used to distinguish the performance characteristics of different module types installed in different climatic zones.

## Acknowledgment

The authors would like to thank PVLab researchers at the University of Applied Sciences and Arts of Southern Switzerland (SUPSI) who have contributed to the outdoor setup and indoor characterization of the PV modules and Solar Durability and Lifetime Extension (SDLE) Research Center researchers at the Case Western Reserve University (CWRU) who have contributed to the ddiv and SunsVoc package developments.

## References

[1] IEA, "Renewables 2020: Analysis and Forecast to 2025," Paris, France, International Energy Agency, Tech. Rep., Nov. 2020. [Online]. Available: https://www.iea.org/reports/renewables-2020

[2] M. Tabakovic, H. Fechner, W. van Sark, A. Louwen, G. Georghiou, G. Makrides, E. Loucaidou, M. Ioannidou, I. Weiss, S. Arancon, and S. Betz, "Status and Outlook for Building Integrated Photovoltaics (BIPV) in Relation to Educational needs in the BIPV Sector," *Energy Procedia*, vol. 111, pp. 993–999, Mar. 2017. [Online]. Available: https://linkinghub.elsevier.com/retrieve/pii/S1876610217302953

[3] E. Biyik, M. Araz, A. Hepbasli, M. Shahrestani, R. Yao, L. Shao, E. Essah, A. C. Oliveira, T. del Caño, E. Rico, J. L. Lechón, L. Andrade, A. Mendes, and Y. B. Atlı, "A key review of building integrated photovoltaic (BIPV) systems," *Engineering Science and Technology, an International Journal*, vol. 20, no. 3, pp. 833–858, Jun. 2017. [Online]. Available: https://linkinghub.elsevier.com/retrieve/pii/S2215098616309326

[4] G. Y. Palacios-Jaimes, P. Martín-Ramos, F. J. Rey-Martínez, and I. A. Fernández-Coppel, "Transformation of a University Lecture Hall in Valladolid (Spain) into a NZEB: LCA of a BIPV System Integrated in Its Façade," *International Journal of Photoenergy*, vol. 2017, pp. 1–11, 2017. [Online]. Available: https://www.hindawi.com/journals/ijp/2017/2478761/

[5] T. Zhang, M. Wang, and H. Yang, "A Review of the Energy Performance and Life-Cycle Assessment of Building-Integrated Photovoltaic (BIPV) Systems," *Energies*, vol. 11, no. 11, p. 3157, Nov. 2018. [Online]. Available: http://www.mdpi.com/1996-1073/11/11/3157

[6] O. Dupré, R. Vaillon, and M. A. Green, *Thermal Behavior of Photovoltaic Devices*. Cham: Springer International Publishing, 2017. [Online]. Available: http://link.springer.com/10.1007/978-3-319-49457-9

[7] D. C. Jordan, C. Deline, M. Deceglie, T. J. Silverman, and W. Luo, "PV Degradation – Mounting & Temperature," in *2019 46th IEEE Photovoltaic Specialists Conference (PVSC)*. Chicago, IL: IEEE, Jun. 2019. [Online]. Available: https://doi.org/10.1109/PVSC40753.2019.8980767

[8] S. Lindig, I. Kaaya, K.-A. Weis, D. Moser, and M. Topic, "Review of Statistical and Analytical Degradation Models for Photovoltaic Modules and Systems as Well as Related Improvements," *IEEE Journal of Photovoltaics*, vol. 8, no. 6, pp. 1773–1786, Nov. 2018. [Online]. Available: https://ieeexplore.ieee.org/document/8472886/

[9] A. J. Curran, C. Birk Jones, S. Lindig, J. Stein, D. Moser, and R. H. French, "Performance Loss Rate Consistency and Uncertainty Across Multiple Methods and Filtering Criteria," in *2019 IEEE 46th Photovoltaic Specialists Conference (PVSC)*, Jun. 2019, pp. 1328–1334, iSSN: 0160-8371.

[10] W. Luo, Y. S. Khoo, P. Hacke, D. Jordan, L. Zhao, S. Ramakrishna, A. G. Aberle, and T. Reindl, "Analysis of the Long-Term Performance Degradation of Crystalline Silicon Photovoltaic Modules in Tropical Climates," *IEEE Journal of Photovoltaics*, vol. 9, no. 1, pp. 266–271, Jan. 2019. [Online]. Available: https://doi.org/10.1109/JPHOTOV.2018.2877007

[11] A. Cuevas and R. A. Sinton, "Prediction of the open-circuit voltage of solar cells from the steady-state photoconductance," *Progress in Photovoltaics: Research and Applications*, vol. 5, no. 2, pp. 79–90, 1997. [Online]. Available: https://doi.org/10.1002/(SICI)1099-159X(199703/04)5:2⟨79::AID-PIP155⟩3.0.CO;2-J

[12] M. J. Kerr, A. Cuevas, and R. A. Sinton, "Generalized analysis of quasi-steady-state and transient decay open circuit voltage measurements," *Journal of Applied Physics*, vol. 91, no. 1, pp. 399–404, Dec. 2001, publisher: American Institute of Physics. [Online]. Available: https://aip.scitation.org/doi/10.1063/1.1416134

[13] A. Cuevas and J. Tan, "Analytical and computer modelling of suns–Voc silicon solar cell characteristics," *Solar Energy Materials and Solar Cells*, vol. 93, no. 6, pp. 958–960, Jun. 2009. [Online]. Available: http://www.sciencedirect.com/science/article/pii/S0927024808004248

[14] F. Recart, H. Mackel, A. Cuevas, and R. Sinton, "Simple Data Acquisition of the Current-Voltage and Illumination-Voltage Curves of Solar Cells1," in *2006 IEEE 4th World Conference on Photovoltaic Energy Conference*, vol. 1, May 2006, pp. 1215–1218, iSSN: 0160-8371.

[15] P. R. Ortega, J. M. Piñol, I. Martín, A. Orpella, G. Masmitjá, G. López, E. Ros, C. Voz, J. Puigdollers, and R. Alcubilla, "Low-cost high-sensitive Suns-Voc measurement instrument to characterize c-Si solar cells," *IEEE Transactions on Instrumentation and Measurement*, pp. 1–1, 2020, conference Name: IEEE Transactions on Instrumentation and Measurement.

[16] T. Roth, J. Hohl-Ebinger, D. Grote, E. Schmich, W. Warta, S. W. Glunz, and R. A. Sinton, "Illumination-induced errors associated with suns-VOC measurements of silicon solar cells," *Review of Scientific Instruments*, vol. 80, no. 3, p. 033106, Mar. 2009, publisher: American Institute of Physics. [Online]. Available: https://aip.scitation.org/doi/full/10.1063/1.3095441

[17] M. K. Forsyth, M. Mahaffey, A. L. Blum, W. A. Dobson, and R. A. Sinton, "Use of the Suns-Voc for diagnosing outdoor arrays modules," in *2014 IEEE 40th Photovoltaic Specialist Conference (PVSC)*, Jun. 2014, pp. 1928–1931, iSSN: 0160-8371.

[18] K. Rühle, M. K. Juhl, M. D. Abbott, and M. Kasemann, "Evaluating Crystalline Silicon Solar Cells at Low Light Intensities Using Intensity-Dependent Analysis of I–V Parameters," *IEEE Journal of Photovoltaics*, vol. 5, no. 3, pp. 926–931, May 2015, conference Name: IEEE Journal of Photovoltaics.

[19] X. Sun, R. V. K. Chavali, and M. A. Alam, "Real-time monitoring and diagnosis of photovoltaic system degradation only using maximum power point—the Suns-Vmp method," *Progress in Photovoltaics: Research and Applications*, vol. 27, no. 1, pp. 55–66, 2019, _eprint: https://onlinelibrary.wiley.com/doi/pdf/10.1002/pip.3043. [Online]. Available: https://onlinelibrary.wiley.com/doi/abs/10.1002/pip.3043

[20] J. Liu, M. Wang, A. J. Curran, A. Maroof Karimi, W.-h. Huang, E. Schnabel, M. Köhl, J. L. Braid, and R. H. French, "Real-world PV Module Degradation across Climate Zones Determined from Suns-Voc, Loss Factors and I-V Steps Analysis of Eight Years of I-V, Pmp Time-series Datastreams," in *2019 IEEE 46th Photovoltaic Specialists Conference (PVSC)*, Jun. 2019, pp. 0680–0686, iSSN: 0160-8371.

[21] M. Wang, J. Liu, T. J. Burleyson, E. J. Schneller, K. O. Davis, R. H. French, and J. L. Braid, "Analytic Isc–Voc Method and Power Loss Modes From Outdoor Time-Series I–V Curves," *IEEE Journal of Photovoltaics*, pp. 1–10, 2020. [Online]. Available: https://ieeexplore.ieee.org/document/9121299/

[22] M. Wang, T. J. Burleyson, J. Liu, A. J. Curran, A. Gok, E. J. Schneller, K. O. Davis, J. L. Braid, and R. H. French, "SunsVoc: Constructing Suns-Voc from Outdoor Time-Series I-V Curves," Oct. 2020. [Online]. Available: https://CRAN.R-project.org/package=SunsVoc

[23] A. Gok, E. Ozkalay, G. Friesen, and F. Frontini, "The Influence of Operating Temperature on the Performance of BIPV Modules," *IEEE Journal of Photovoltaics*, vol. 10, no. 5, pp. 1371–1378, Sep. 2020. [Online]. Available: https://ieeexplore.ieee.org/document/9119434/

[24] W.-H. Huang, X. Ma, J. Liu, A. J. Curran, J. S. Fada, J.-N. Jaubert, J. Sun, J. L. Braid, J. Brynjarsdottir, and R. H. French, "ddiv: Data Driven I-v Feature Extraction," Sep. 2018. [Online]. Available: https://CRAN.R-project.org/package=ddiv

[25] X. Ma, W.-H. Huang, E. Schnabel, M. Köhl, J. Brynjarsdóttir, J. L. Braid, and R. H. French, "Data-Driven I–V Feature Extraction for Photovoltaic Modules," *IEEE Journal of Photovoltaics*, vol. 9, no. 5, pp. 1405–1412, Sep. 2019, conference Name: IEEE Journal of Photovoltaics.

[26] J. A. Kratochvil, W. E. Boyson, and D. L. King, "Photovoltaic array performance model," Sandia National Laboratories, United States, Tech. Rep. SAND2004-3535, Aug. 2004. [Online]. Available: https://doi.org/10.2172/919131

[27] E. Hasselbrink, M. Anderson, Z. Defreitas, M. Mikofski, Y. Shen, S. Caldwell, A. Terao, D. Kavulak, Z. Campeau, and D. DeGraaff, "Validation of the PVLife model using 3 million module-years of live site data," in *2013 IEEE 39th Photovoltaic Specialists Conference (PVSC)*, Jun. 2013, pp. 0007–0012. [Online]. Available: https://doi.org/10.1109/PVSC.2013.6744087

[28] D. C. Jordan, C. Deline, S. R. Kurtz, G. M. Kimball, and M. Anderson, "Robust PV Degradation Methodology and Application," *IEEE Journal of Photovoltaics*, vol. 8, no. 2, pp. 525–531, Mar. 2018. [Online]. Available: https://doi.org/10.1109/JPHOTOV.2017.2779779

[29] D. C. Jordan and S. R. Kurtz, "Photovoltaic Degradation Rates—an Analytical Review," *Progress in Photovoltaics: Research and Applications*, vol. 21, no. 1, pp. 12–29, Jan. 2013. [Online]. Available: http://onlinelibrary.wiley.com/doi/10.1002/pip.1182/abstract

[30] V. Reinöhl, J. Sedlář, and M. Navrátil, "Photo-oxidation of poly(vinylbutyral)," *Polymer Photochemistry*, vol. 1, no. 3, pp. 165–175, Jul. 1981. [Online]. Available: http://www.sciencedirect.com/science/article/pii/0144288081900178

[31] M. Koehl, S. Hamperl, and M. Heck, "Effect of thermal insulation of the back side of PV modules on the module temperature," *Progress in Photovoltaics: Research and Applications*, vol. 24, no. 9, pp. 1194–1199, 2016. [Online]. Available: https://onlinelibrary.wiley.com/doi/abs/10.1002/pip.2773

[32] S. W. Glunz, S. Rein, J. Y. Lee, and W. Warta, "Minority carrier lifetime degradation in boron-doped Czochralski silicon," *Journal of Applied Physics*, vol. 90, no. 5, pp. 2397–2404, Sep. 2001. [Online]. Available: http://aip.scitation.org/doi/10.1063/1.1389076

[33] J. Lindroos and H. Savin, "Review of light-induced degradation in crystalline silicon solar cells," *Solar Energy Materials and Solar Cells*, vol. 147, pp. 115–126, Apr. 2016. [Online]. Available: http://www.sciencedirect.com/science/article/pii/S0927024815006406

[34] K. Lee, M.-S. Kim, J.-K. Lim, J.-H. Ahn, M.-I. Hwang, and E.-C. Cho, "Natural Recovery from LID: Regeneration under Field Conditions?" *31st European Photovoltaic Solar Energy Conference and Exhibition; 1835-1837*, 2015. [Online]. Available: http://www.eupvsec-proceedings.com/proceedings?paper=33519

[35] M. D. Kempe, G. J. Jorgensen, K. M. Terwilliger, T. J. McMahon, C. E. Kennedy, and T. T. Borek, "Acetic acid production and glass transition concerns with ethylene-vinyl acetate used in photovoltaic devices," *Solar Energy Materials and Solar Cells*, vol. 91, no. 4, pp. 315–329, Feb. 2007. [Online]. Available: http://www.sciencedirect.com/science/article/pii/S0927024806004107

[36] M. D. Kempe, D. C. Miller, J. H. Wohlgemuth, S. R. Kurtz, J. M. Moseley, Q. A. Shah, G. Tamizhmani, K. Sakurai, M. Inoue, T. Doi, A. Masuda, S. L. Samuels, and C. E. Vanderpan, "Field testing of thermoplastic encapsulants in high-temperature installations," *Energy Science & Engineering*, vol. 3, no. 6, pp. 565–580, 2015. [Online]. Available: https://onlinelibrary.wiley.com/doi/abs/10.1002/ese3.104

[37] A. Dhaliwal and J. Hay, "The characterization of polyvinyl butyral by thermal analysis," *Thermochimica Acta*, vol. 391, no. 1-2, pp. 245–255, Aug. 2002. [Online]. Available: https://linkinghub.elsevier.com/retrieve/pii/S0040603102001879